Proteome-wide autoantibody screening and holistic autoantigenomic analysis unveil COVID-19 signature of autoantibody landscape

Kazuki M Matsuda, MD, PhD,[1*] Yoshiaki Kawase, PhD,[2*] Kazuhiro Iwadoh, MD, PhD,[1] Makoto Kurano, MD, PhD,[3] Yutaka Yatomi, MD, PhD,[4] Koh Okamoto, MD, MS, PhD,[5] Kyoji Moriya, MD, PhD,[5,6] Hirohito Kotani,[1] MD, PhD,[1] Teruyoshi Hisamoto, MD, PhD,[1] Ai Kuzumi, MD, PhD[1], Takemichi Fukasawa MD, PhD[1,7], Asako Yoshizaki-Ogawa, MD, PhD[1], Masanori Kono, MD, PhD,[8] Tomohisa Okamura, MD, PhD, [8] Hirofumi Shoda, MD, PhD, [8] Keishi Fujio, MD, PhD, [8] Kei Yamaguchi, PhD, [9] Taishi Okumura,[9] Chihiro Ono,[9] Yuki Kobayashi, PhD,[9] Ayaka Sato,[9] Ayako Miya,[9] PhD, Naoki Goshima, PhD, [9] Rikako Uchino,[10] Yumi Murakami, PhD,[10] Hiroshi Matsunaka, PhD,[10] Hiroshi Imai, PhD, [2] Shinichi Sato, MD, PhD, [1] Rudy Raymond, PhD, [2] Ayumi Yoshizaki, MD, PhD[1,7#]

1. Department of Dermatology, The University of Tokyo Graduate School of Medicine, Tokyo, Japan
2. Department of Computer Science, The University of Tokyo Graduate School of Information Science and Technology, Tokyo, Japan

3. Department of Clinical Laboratory Medicine, The University of Tokyo Graduate School of Medicine, Tokyo, Japan

4. Graduate School, International University of Health and Welfare, Tokyo, Japan

5. Department of Infectious Diseases, The University of Tokyo Hospital, Tokyo, Japan

6. Division of Infection Prevention and Control, Postgraduate School of Healthcare, Tokyo Healthcare University, Tokyo, Japan

7. Department of Clinical Cannabinoid Research, The University of Tokyo Graduate School of Medicine, Tokyo, Japan

8. Department of Allergy and Rheumatology, The University of Tokyo Graduate School of Medicine, Tokyo, Japan

9. ProteoBridge Corporation, Tokyo, Japan

10. NOV Academic Research, TOKIWA Pharmaceutical Co., Ltd., Tokyo, Japan

* Equally contributed.

 # Corresponding authors

Ayumi Yoshizaki, MD, PhD

Department of Dermatology and Department of Clinical Cannabinoid Research, The University of Tokyo Graduate School of Medicine, 7-3-1, Hongo, Bunkyo-ku, Tokyo, Japan, 1138655

Phone: +81-3-3815-5411

ORCID: 0000-0002-8194-9140

E-mail: ayuyoshi@me.com

Abstract

This study presents “aUToAntiBody Comprehensive Database (UT-ABCD)”, a proteome-wide catalog of autoantibody profiles in 284 human individuals. The subjects included patients diagnosed with Coronavirus disease 2019 (COVID-19), systemic sclerosis (SSc), systemic lupus erythematosus (SLE), anti-neutrophil cytoplasmic antibody-associated vasculitis (AAV), atopic dermatitis (AD), as well as healthy controls (HC). Our investigation employed proteome-wide autoantibody screening (PWAS) that utilizes 13,350 autoantigens displayed on wet protein arrays, covering approximately 90% of the human transcriptome. Our findings demonstrated significant elevation of autoantibody levels in COVID-19, SSc, and SLE patients. Unique sets of disease-specific autoantibodies were identified, highlighting the role of autoantibodies against proteins associated with cytokine signaling in immune systems and viral infection pathways. Employing machine learning, we distinguished COVID-19 cases with high accuracy based on autoantibody profiles, notably identifying antibodies against proteins encoded by *BCORP1* and *KAT2A* as highly specific to COVID-19. Longitudinal analysis revealed dynamic changes in autoantibody levels throughout the course of COVID-19, independent of disease severity. Our research highlights the effectiveness of integrating PWAS and autoantigenomics in exploring immune

responses in COVID-19 and other diseases. It provides a deeper understanding of the autoimmunity landscape in human disorders and introduces a new bioresource for further investigation.

Introduction

Coronavirus disease 2019 (COVID-19), an infectious disease caused by severe acute respiratory syndrome coronavirus 2 (SARS-CoV-2),[1] has brought a global pandemic since early 2020 with threat on human health and public safety throughout the world.[2] The pathophysiology of COVID-19 is characterized by multiple organ injuries triggered by excessive immune response.[3,4] Cytokine storm in the lung causes acute respiratory distress syndrome, which leads to hypoxemia, respiratory failure, requirement of ventilation, and even death. One of the biggest challenges in clinical management of COVID-19 patients lies in accurately identifying and categorizing cases at higher risk of such serious clinical course. Known risk factors include older age, male gender, smoking, diabetes, obesity, hypertension, immunodeficiency, and malignancies.[5]

Humoral immunity plays pivotal roles in COVID-19. Although dramatic success of mRNA vaccines and SARS-CoV-2 neutralizing monoclonal antibodies in preventing serious illnesses, accumulating evidence have suggested the vicious roles of dysregulated humoral immunity. As well as earlier work linking anti-cytokine antibodies to mycobacterial, staphylococcal and fungal diseases,[6,7] autoantibodies against cytokines have been described in COVID-19.[8] Especially, anti-type I Interferon

antibodies distinguished ~10% of life-threatening pneumonia and ~20% of deaths from COVID-19.[9–11] A high-throughput screening by yeast display of the secretome further revealed the presence of autoantibodies against several immune factors, including chemokines.[12] In addition, autoantibodies characteristic of systemic autoimmune disorders, such as anti-phospholipid antibodies, anti-nuclear antibodies and rheumatoid factor, were reported in COVID-19.[13] More recently, association between COVID-19 severity and autoantibodies targeting G protein-coupled receptors and renin-angiotensin system-related proteins has been reported.[14]

To comprehensively understand such clinical significance of autoantibodies in human diseases including COVID-19, high-precision autoantibody measurement with a proteome-wide scale is necessary. Herein, we engaged our unique technology for proteome-wide autoantibody screening (PWAS) that covers approximately 90% of the human transcriptome,[15–17] in the serum samples derived from individual patients. Our pipeline integrates human cDNA library (HuPEX),[18] a wheat germ cell-free system for high-throughput *in vitro* protein synthesis,[19–21] and technology for manipulating protein arrays kept in moist conditions during the entire handling process,[22] namely wet protein arrays (WPAs). We have applied this method in multiple inflammatory or malignant disorders for validating its potential for illustrating the “autoantibody landscape” of

102 human disorders, which revealed its usefulness for holistic evaluation of disease-related
103 autoantibodies,[17] developing novel biomarkers,[15] and moreover, investigating unknown
104 pathophysiology driven by autoantibodies.[16]

105 Our aim was to demonstrate the utility of our omics-based methodology for
106 autoantibody evaluation and data interpretation procedure, so-called "autoantigenomics,"
107 targeting COVID-19. In 2020, Moritz *et al.* defined autoantigenomics as a branch of
108 systems immunology, which holistically analyze the repertoire of autoantibodies
109 engaging omics-based bioinformatical approaches including hierachical cluster analysis,
110 enrichment analysis, and machine learning.[23] The concept of autoantigenomics stand on
111 hypotheses that there might be differences in the sets of targeted antigens underlying
112 intra-disease heterogeneity in human, which would be supported by our novel data
113 shown below.
114

Results

Overview

We recruited 73 patients with COVID-19, 32 patients with systemic sclerosis (SSc), 60 patients with systemic lupus erythematosus (SLE), 29 patients with anti-neutrophil cytoplasmic antibody-associated vasculitis (AAV), 26 patients with atopic dermatitis (AD), and 64 healthy controls (HC) for serum sample collection (**Supplementary Table 1**). For each individual serum, PWAS was performed (**Fig. 1**). The digest of the results will be available as "aUToAntiBody Comprehensive Database (UT-ABCD)". We found that sum of autoantibody levels (SAL) was significantly elevated in patients with COVID-19, SSc, or SLE, compared to HCs, while there was no statistically significant difference in SAL between AD or AAV patients and HCs (**Fig. 2A**). This tendency was consistent across both gender and age groups. (**Supplementary Fig. 1**).

Identification of disease-specific autoantibodies

We identified distinct sets of autoantibodies that showed a more than twofold significant increase in each disease condition relative to HCs (**Fig. 2B**). Notably, certain autoantibodies were unique to each disease (**Fig. 2C**). To illustrate the variability in

serum levels of these disease-specific autoantibodies across individuals, we utilized uniform manifold approximation and projection (UMAP), resulting in distinctive patterns on the UMAP plots for each condition (**Fig. 2D**). Gene ontology analysis linked to the genes responsible for the proteins targeted by such disease-specific autoantibodies pointed to shared biological functions, with a focus on viral infection pathways and cytokine signaling in immune system, in COVID-19, SLE, and AAV (**Fig. 2E and 2F**). Holistic analysis of autoantibodies targeting cytokines, or their receptors displayed on our WPAs revealed that strong positivity for autoantibodies targeting type 1 interferon was specifically observed in COVID-19 patients, while weak positivity was seen in SLE patients (**Supplementary Fig. 2**).

Selection of machine learning frameworks

To further investigate the association between autoantibody profiles and COVID-19, we adopted a machine learning approach. We tested nine different methods to differentiate COVID-19 cases from the others: simple linear regression, Ridge regression, logistic regression with data normalization, logistic regression with data standardization, support vector machine with data normalization, support vector machine with data standardization, light gradient boosting machine (LightGBM), and

151 extremely gradient boosting decision trees (XGBoost). As a result, XGBoost showed
152 the highest value of the area under the receiver-operator characteristics curve for
153 distinction of COVID-19 cases from the others (**Supplementary Table 2**).
154 Consequently, we opted to focus on this method for our subsequent analysis.

155

156 *Performance of XGBoost*

157 In our subsequent analysis using the entire dataset, we experimented with
158 binary (COVID-19 vs. others), ternary (mild COVID-19 vs. moderate to severe
159 COVID-19 vs. others), and multiclass (mild COVID-19 vs. moderate to severe
160 COVID-19 vs. AAV vs. AD vs. SSc vs. SLE vs. HCs) classifications through XGBoost.
161 The most significant autoantibodies identified across all models are depicted in **Fig. 3A,**
162 **3B, and 3C**, with autoantibodies against translational products from *BCL6 Corepressor*
163 *Pseudogene 1* (*BCORP1*) emerging as a top feature in every model. Similarly,
164 antibodies against K-Acetyltransferase 2A (KAT2A) were consistently prominent.
165 Notably, Anti-BCORP1 and anti-KAT2A Abs were highlighted as important items in
166 all the candidate machine learning methods tested (**Supplementary Fig. 3**). There was a
167 correlation between anti-BCORP Abs and anti-KAT2A Abs as illustrated in **Fig. 3D,**
168 **3E, and 3F**. Remarkably, established serum markers for SSc and SLE, such as

anti-topoisomerase 1 (TOP1) Abs, anti-centromere protein-B (CENPB) Abs, anti-tripartite motif-containing protein 21 (TRIM21) Abs, anti-small nuclear ribonucleoprotein polypeptide (SNRP)-A Abs, and anti-SNRPB Abs, were also identified. The visualization of mean serum levels of these prominent markers through spider charts revealed distinctive patterns across the different conditions (**Fig. 3G, 3H, and 3I**). The models incorporating these markers as features achieved the highest accuracy in both binary and ternary classifications and showed significantly better outcomes than chance in the complex seven-class classification (**Supplementary Table 3**).

Clinical relevance of autoantibodies

The serum levels of the top 20 autoantibodies highlighted through multi-class classification for each participant were depicted in a heatmap (**Fig. 4A**). Hierarchical clustering identified three unique groups of autoantibodies: cluster I, which included two autoantibodies highly specific to COVID-19 (anti-BCORP1 and anti-KAT2A Abs); cluster II, comprising autoantibodies that are commonly elevated across various conditions; and cluster III, involving well-established biomarkers for SSc and SLE. Principal component analysis (PCA) effectively distinguished between seven categories

(**Fig. 4B**), particularly using principal component (PC) 2 as an indicator for COVID-19 (**Fig. 4C**). Correspondingly, antibodies against BCORP1 and KAT2A constituted the predominant contribution to PC2 (**Fig. 4D**). Serum levels of anti-BCORP1 and anti-KAT2A Abs were prominently elevated in COVID-19, along with a part of cases with SLE (**Fig. 4E and 4F**). This trend was consistent among both sex and age groups (**Supplementary Fig. 4**). We also explored the link between COVID-19 clinical outcomes and the presence of anti-BCORP1 or anti-KAT2A Abs. Applying a threshold set at the mean plus two standard deviations above healthy controls (indicated by the red dashed lines in **Fig. 4B and 4C**), we identified 61 of the 73 total COVID-19 cases as having elevated levels of anti-BCORP1Abs and 34 cases with elevated levels of anti-KAT2A Abs. While no significant association was found between elevated anti-BCORP1 Abs and clinical features (**Supplementary Table 4**), elevation of anti-KAT2A Abs was significantly linked to a reduced need for intensive care, including intubation and mechanical ventilation (odds ratio = 0.19, P = 0.02; **Supplementary Table 5**).

Time course of autoantibody levels during COVID-19

Finally, we conducted longitudinal analysis of the humoral immune response in COVID-19 patients targeting paired serum samples from an "early" timepoint (within 10 days after symptoms began) and a "late" timepoint (11-20 days after symptom onset) from 41 individuals. These samples were used for PWAS and for assessing IgG levels against SARS-CoV-2 particles: the nucleocapsid protein (N), spike protein (S), and the receptor binding domain (RBD) of S. Consistent with our prior findings, early timepoint samples showed IgG against N, S, and RBD in only a small part of the patients, with a marked increase in most patients by the late timepoint (**Fig. 5A**). To the contrary, SAL remained unchanged over time (**Fig. 5B**). Further exploration revealed a significant decrease in 293 autoantibodies and increase in 116 autoantibodies over the course of the infection, including those targeting BCORP1 and KAT2A (**Fig. 5C and 5D**). There was no observed correlation between these autoantibodies and IgG levels against N, S, and RBD (**Fig. 5E**). Notably, both anti-BCORP1 and anti-KAT2A Ab levels rose over time independent of disease severity (**Fig. 5F**). Additional analysis did not find any correlation between these two autoantibodies and IgG targeting N, S, and RBD at either timepoint or their progression over time (**Fig. 5G and 5H**).

Discussion

Herein we conducted PWAS subjecting serum samples derived from HCs and patients with COVID-19, AD, AAV, SLE, and SSc (**Fig. 1**). We demonstrated that our PWAS methodology enables us to identify disease-specific autoantibodies (**Fig. 2A, 2B, and 2C**), which demonstrate the distinct distribution of autoantibodies and common biological processes among different conditions (**Fig. 2D, 2E, and 2F**). The contrast in autoantibody profiles was accentuated through the application of a machine learning approach, particularly leveraging the XGBoost framework (**Fig. 3 and 4**). We also investigated the longitudinal change of autoantibody profiles along with the time course of COVID-19 and its correlation with emergence of antibodies targeting COVID-19 particles (**Fig. 5**). Collectively, these results supported our hypothesis that the combination of PWAS and omics-based bioinformatic methodologies is adaptable to human disorders including COVID-19. Additionally, our findings in this study as well as our previous works provide a comprehensive catalog of autoantibody profiles in various diseases and open the door to creating innovative diagnostic methods that can differentiate between various disease mechanisms affecting multiple organs, utilizing distinct autoantibody patterns measured by WPAs.[15,17]

The machine learning-based approach has discovered that the presence of anti-BCORP1 antibodies is highly specific to COVID-19 (**Fig. 4E**). Despite *BCORP1* being categorized as a pseudogene, it appears to undergo transcription into mRNA, as several transcriptomic studies have reported the presence of *BCORP1*-derived sequences.[24,25] Especially, Deng MC's research has shown that the transcription levels of *BCORP1* in peripheral blood mononuclear cells of COVID-19 patients correlate with early functional recovery and 1-year survival.[25] However, it remains unclear whether *BCORP1* mRNA is translated into functional proteins, and further investigation is needed in this regard. Moreover, our discovery of anti-BCORP1 Abs in both males and females raises questions, as BCORP1 is located on the Y chromosome. This leads us to consider the possibility of cross-reactivity of these antibodies against foreign antigens, such as proteins comprising SARS-CoV-2 virions. However, we could not find any correlation between serum levels of anti-BCORP1 Abs and antibodies targeting SARS-CoV-2 particles at any of the timepoints examined, nor in their changes over time (**Fig. 5G**). Another hypothesis is cross-reaction between the antigen we produced from *BCORP1* cDNA and other human proteins. The *BCL2 co-repressor* (*BCOR*) gene, the counterpart of *BCORP1* found on the X chromosome, has a nucleotide sequence that is over 99% identical to *BCORP1*. It is conceivable that the BCOR protein is the actual

target of the detected anti-BCORP1 Abs in our study. However, this theory remains unconfirmed as our cDNA library did not include *BCOR* cDNA to validate this hypothesis.

Anti-KAT2A antibodies were also found to be specifically elevated in the sera of COVID-19 patients (**Fig. 4F**). Like anti-BCORP1 Abs, the levels of anti-KAT2A Abs increased over the course of COVID-19 but were not correlated to antibodies targeting SARS-CoV-2 particles (**Fig. 5H**). This observation indicates that autoantibodies to KAT2A emerge because of autoantigen exposure due to tissue damage triggered by COVID-19, not as a reflection of cross-reaction between SARS-CoV-2 virions. KAT2A functions as a histone acetyltransferase that plays a role in the epigenetic regulation of the genome by modifying chromatin structures. There is notable research by John K. et al., indicating that the SARS-CoV-2 ORF8 protein mimics the histone H3's ARKS motifs, which interfere with the role of KAT2A role in host cell epigenetic regulation.[26] Intriguingly, patients who did not show an increase in anti-KAT2A antibodies were more often those requiring intensive care and mechanical ventilation (**Supplementary Table 5**). This observation has led to the proposition that the presence of anti-KAT2A Abs could be indicative of an effective immune response to the virus by KAT2A upregulation, a hypothesis that warrants further research.

Our study has multiple strengths. First, the wheat-germ *in vitro* protein synthesis system and technique for manipulation of WPAs realized high-throughput expression of various human proteins including exoproteome upon a single platform. Second, as a result, our autoantibody measurement could cover a wider range of antigens at an almost proteome-wide level, which enabled us to apply omics-based bioinformatical approaches for interpreting the data. Third, we investigated the longitudinal change of autoantibody profiles within COVID-19 patients, along with the measurement of antibodies targeting SARS-CoV-2 particles. The limitation of our present study includes its retrospective design and a relatively small number of the subjects. Furthermore, we could not distinguish whether the autoantibodies found in our measurement were predisposed before COVID-19 or newly appeared after infection. In addition, functional assays for the autoantibodies such as neutralizing assays or *in vivo* studies are lacking. Therefore, insights into the direct contribution of each autoantibody to the pathophysiology of COVID-19 are limited. Our next challenges would include collecting serum samples before and after COVID-19 by accessing to population-based cohorts, evaluating the function of each autoantibody against their target molecules, and testing their contribution to the pathogenesis in animal experiments.

References

1. Grp, C. S. & Version, P. The species Severe acute respiratory syndromerelated coronavirus: classifying 2019-nCoV and naming it SARS-CoV-2. *Nat. Microbiol.* **5**, 5346–544 (2020).

2. Hu, B., Guo, H., Zhou, P. & Shi, Z.-L. Characteristics of SARS-CoV-2 and COVID-19. *Nat. Rev. Microbiol.* **19**, 141–154 (2021).

3. Mehta, P. *et al.* COVID-19: consider cytokine storm syndromes and immunosuppression. *Lancet* **295**, 1033–1034 (2020).

4. Huang, C. *et al.* Clinical features of patients infected with 2019 novel coronavirus in Wuhan , China. *Lancet* **395**, 497–506 (2020).

5. Dessie, Z. G. & Zewotir, T. Mortality□related risk factors of COVID□19: a systematic review and meta□analysis of 42 studies and 423,117 patients. *BMC Infect. Dis.* **21**, 855 (2021).

6. Puel, A., Bastard, P., Bustamante, J. & Casanova, J.-L. Human autoantibodies underlying infectious diseases. *J. Exp. Med.* **219**, e20211387 (2022).

7. Cheng, A. & Holland, S. M. Anti-cytokine autoantibodies: mechanistic insights and disease associations. *Nat. Rev. Immunol.* (2023) doi:10.1038/s41577-023-00933-2.

8. Muri, J. *et al.* Autoantibodies against chemokines post-SARS-CoV-2 infection correlate with disease course. *Nat. Immunol.* **24**, 604–611 (2023).

9. Bastard, P. *et al.* Autoantibodies against type I IFNs in patients with life-threatening COVID-19. *Science (80-.).* **370**, (2020).

10. Bastard, P. *et al.* Autoantibodies neutralizing type I IFNs are present in ~4% of uninfected individuals over 70 years old and account for ~20% of COVID-19 deaths. *Sci. Immunol.* **6**, (2021).

11. Eto, S. *et al.* Neutralizing Type I Interferon Autoantibodies in Japanese Patients with Severe COVID-19. *J. Clin. Immunol.* **42**, 1360–1370 (2022).

12. Wang, E. Y. *et al.* Diverse functional autoantibodies in patients with COVID-19. *Nature* **595**, 283–288 (2021).

13. Chang, S. E. *et al.* New-onset IgG autoantibodies in hospitalized patients with COVID-19. *Nat. Commun.* **12**, 5417 (2021).

14. Cabral-marques, O. *et al.* Autoantibodies targeting GPCRs and RAS-related molecules associate with COVID-19 severity. *Nat. Commun.* **13**, 1220 (2022).

15. Matsuda, K. M. *et al.* Autoantibody Landscape Revealed by Wet Protein Array□: Sum of Autoantibody Levels Re fl ects Disease Status. *Front. Immunol.* **13**, 1–14 (2022).

16. Matsuda, K. M., Kotani, H., Yamaguchi, K., Okumura, T. & Fukuda, E. Significance of anti-transcobalamin receptor antibodies in cutaneous arteritis revealed by proteome-wide autoantibody screening. *J. Autoimmun.* **135**, 102995 (2023).

17. Kuzumi, A. *et al.* Comprehensive autoantibody profiling in systemic autoimmunity by a highly-sensitive multiplex protein array. *Front. Immunol.* **14**, (2023).

18. Goshima, N. *et al.* Human protein factory for converting the transcriptome into an in vitro-expressed proteome. *Nat. Methods* **5**, 1011–1017 (2008).

19. Sawasaki, T., Ogasawara, T., Morishita, R. & Endo, Y. A cell-free protein synthesis system for high-throughput proteomics. *Proc. Natl. Acad. Sci. U. S. A.* **99**, 14652–14657 (2002).

20. Sawasaki, T. *et al.* A bilayer cell-free protein synthesis system for high-throughput screening of gene products. *FEBS Lett.* **514**, 102–105 (2002).

21. Endo, Y. & Sawasaki, T. Cell-free expression systems for eukaryotic protein production. *Curr. Opin. Biotechnol.* **17**, 373–380 (2006).

344 22. Fukuda, E. *et al.* Identification and characterization of the antigen recognized by
345 the germ cell mAb TRA98 using a human comprehensive wet protein array.
346 *Genes to Cells* **26**, 180–189 (2021).
347 23. Moritz, C. P. *et al.* Autoantigenomics: Holistic characterization of autoantigen
348 repertoires for a better understanding of autoimmune diseases. *Autoimmun. Rev.*
349 **19**, 102450 (2020).
350 24. Fagerberg, L. *et al.* Analysis of the human tissue-specific expression by
351 genome-wide integration of transcriptomics and antibody-based proteomics. *Mol.*
352 *Cell. Proteomics* **13**, 397–406 (2014).
353 25. Deng, M. C. Multi-dimensional COVID-19 short- and long-term outcome
354 prediction algorithm. *Expert Rev. Precis. Med. drug Dev.* **5**, 239–242 (2020).
355 26. Kee, J. *et al.* SARS-CoV-2 disrupts host epigenetic regulation via histone
356 mimicry. *Nature* **610**, 381–388 (2022).
357 27. Yamakawa, K. *et al.* Japanese rapid/living recommendations on drug
358 management for COVID □19: updated guidelines (July 2022). *Acute Med. Surg.*
359 **9**, 1–21 (2022).

28. Nakano, Y. *et al.* Time course of the sensitivity and specificity of anti-SARS-CoV-2 IgM and IgG antibodies for symptomatic COVID-19 in Japan. *Sci. Rep.* **11**, 1–10 (2021).

29. Qian, C. *et al.* Development and multicenter performance evaluation of fully automated SARS-CoV-2 IgM and IgG immunoassays. *Clin. Chem. Lab. Med.* **58**, 1601–1607 (2020).

30. Zhou, Y. *et al.* Metascape provides a biologist-oriented resource for the analysis of systems-level datasets. *Nat. Commun.* **10**, 1523 (2019).

Materials and Methods

Human subjects

We consecutively enrolled patients administered to our institution for COVID-19 from April 2020 to April 2021. Inclusion criteria were a SARS-CoV-2 positive nasopharyngeal swab test by real-time reverse transcription-polymerase chain reaction (RT-PCR) and age ≥18 years. Clinical data were collected by retrospective review of electric medical records. We gathered basic patient information, symptoms, medications, histopathologic features, and laboratory findings from the closest time point from the date of serum collection. The disease severity was assessed following the Japanese guideline for managing COVID-19 patients.[27] In brief, individuals requiring intensive care or mechanical ventilation were categorized as severe COVID-19, those exhibiting hypoxemia among the remaining cases were classified as moderate to severe COVID-19, and all other patients were considered to have mild COVID-19. We also gathered serum samples from HCs and patients with AD, AAV, SLE, and SLE. This study has been approved by The University of Tokyo Ethical Committee (Approval number 0695). Written informed consent has been obtained from all the participants.

Measurement of IgG targeting SARS-CoV-2 particles

388 The process of quantifying IgG antibodies that target specific SARS-CoV-2
389 proteins, namely the nucleocapsid protein, spike protein, and the spike protein's
390 receptor binding domain, was conducted as outlined previously using a commercial
391 SARS-CoV-2 IgG kit (YHLO Biotechnology Company, Ltd., Shenzhen, China).[28,29]
392 This involved an assay where serum samples were combined with magnetic beads
393 coated with the viral proteins and a substance to prepare the samples. This mix was then
394 washed, combined with an acridinium-conjugated anti-human IgG, and washed again.
395 The subsequent steps included adding solutions to induce a chemiluminescent reaction,
396 the intensity of which was measured by the iFlash3000 CLIA analyzer (YHLO
397 Biotechnology Company, Ltd.) A threshold of 10 AU/mL was used for the detection,
398 following the guidelines provided by the manufacturer.
399
400 *Autoantibody measurement*
401 WPAs were arranged as previously described.[15] First, proteins were
402 synthesized *in vitro* utilizing a wheat germ cell-free system from 13,350 clones of the
403 HuPEX.[18] Second, synthesized proteins were plotted onto glass plates (Matsunami
404 Glass, Osaka, Japan) in an array format by the affinity between the GST-tag added to
405 the N-terminus of each protein and glutathione modified on the plates. The WPAs were

406 treated with human serum diluted by 3:1000 in the reaction buffer containing 1x
407 Synthetic block (Invitrogen), phosphate-buffered saline (PBS), and 0.1% Tween 20.
408 Next, the WPAs were washed, and goat anti-Human IgG (H+L) Alexa Flour 647
409 conjugate (Thermo Fisher Scientific, San Jose, CA, USA) diluted 1000-fold was added
410 to the WPAs and reacted for 1 hour at room temperature. Finally, the WPAs were
411 washed, air-dried, and fluorescent images were acquired using a fluorescence imager
412 (Amersham Typhoon, Cytiva, Marlborough, MA, USA). Fluorescence images were
413 analyzed to quantify serum levels of autoantibodies targeting each antigen, following
414 the formula shown below:
415

$$Autoantibody\ level\ [AU] = \frac{F_{autoantigen} - F_{negative\ control}}{F_{positive\ control} - F_{negative\ control}} \times 100$$

416 *AU*: arbitrary unit
417 $F_{autoantigen}$: fluorescent intensity of autoantigen spot
418 $F_{negative\ control}$: fluorescent intensity of negative control spot
419 $F_{positive\ control}$: fluorescent intensity of positive control spot
420
421 *Machine learning*

We applied supervised machine learning techniques using the Python code with the scikit-learn library to analyze the measurement data for autoantibodies from 284 patients. At random forest, decision trees were built and trained in parallel on subsets of sampled instances and features. Meanwhile, at XGBoost decision trees were built sequentially to improve each other. The final prediction of the random forest was the majority of its decision trees, while that of XGBoost was from their weighted average. The performance of the classifiers was evaluated in area under the operator-receiver characteristics curve (AUC), accuracy, precision, recall, and F1-score, calculated by 5-fold cross validation. The accuracy is the ratio of the correct positive and negative prediction, the precision is the ratio of the correct positive prediction, the recall (or, sensitivity) is the ratio of the correct positive prediction among all true positive instances, and F1-score is the harmonic mean of precision and sensitivity.

Statistical analysis

Differentially elevated autoantibodies were defined as more than 2-fold changes in the serum levels with a P value < 0.01. Gene Ontology Analysis using web-based tools targeted the list of the entry clones coding the differentially highlighted autoantigens was performed for gene-list enrichment analysis, gene-disease association

440 analysis, and transcriptional regulatory network analysis with Metascape.[30] Other data
441 analyses and presentations were conducted using Stata IC/15.0 (StataCorp, TX, USA).
442
443 *Data visualization*
444 Box plots, scatter plots, hierarchical clustering and correlation matrix were
445 visualized by using R (v4.2.1). Box plots were defined as follows: the middle line
446 corresponds to the median; the lower and upper hinges correspond to the first and third
447 quartiles; the upper whisker extends from the hinge to the largest value no further than
448 1.5 times the interquartile range (IQR) from the hinge; and the lower whisker extends
449 from the hinge to the smallest value at most 1.5 times the IQR of the hinge.
450

Acknowledgements

We thank Ms. Maiko Enomoto and her colleagues for secretary work. We thank Ms. Teruko Tani and Ms. Mayumi Odagiri for their assistance in clinical data collection. We appreciate Ms. Maiko Matsuda, VESPER Studio Inc., Tokyo, Japan, for her contribution of illustrating skills.

Author Contributions

KM Matsuda primarily engaged in autoantibody measurement, clinical data collection, data analysis, visualization, and writing the first draft of the manuscript. Y Kawase primarily contributed to machine learning analysis. K Iwadoh also participated in machine learning analysis. M Kurano, Y Yatomi, K Okamoto, and K Moriya participated in sample collection and clinical data acquisition regarding COVID-19. H Kotani, A Kuzumi, T Fukasawa, A Yoshizaki-Ogawa took part in the sample collection of SSc. T Hisamoto was in charge of sample collection of AD. M Kono, T Okamura, H Shoda, and K Fujio oversaw sample collection of SLE. K Yamaguchi, T Okumura, C Ono, Y Kobayashi, A Sato, A Miya, and N Goshima prepared wet protein arrays, provided technical assistance for autoantibody measurement, participated in data analysis, setup of UT-ABCD, and revised the manuscript. R Uchino, Y Murakami and H Matsunaka provided technical assistance for autoantibody measurement. H Imai and R Raymond supervised the study. S Sato conceptualized and supervised the study. A Yoshizaki conceptualized, launched, and supervised this study, and was involved in revising the manuscript.

Conflict-of-interest statement

K Yamaguchi, T Okumura, C Ono, Y Kobayashi, A Miya, A Sato, and N Goshima were employed by ProteoBridge Corporation. T Fukasawa and A Yoshizaki belong to the Social Cooperation Program, Department of Clinical Cannabinoid Research, The University of Tokyo Graduate School of Medicine, Tokyo, Japan, supported by Japan Cosmetic Association and Japan Federation of Medium and Small Enterprise Organizations. T Okamura belongs to the Social Cooperation Program, Department of Functional Genomics and Immunological Diseases, The University of Tokyo Graduate School of Medicine, Tokyo, Japan, supported by Chugai Pharmaceutical Corporation. The remaining authors declare that the research was conducted in the absence of any commercial or financial relationships that could be construed as a potential conflict of interest.

Figure legends

Figure 1. Scheme of PWAS pipeline.

In the first step, proteins were synthesized *in vitro* from the proteome-wide human cDNA library (HuPEX). Promotors (P), Enhancers (E), and FLAG-GST tags were fused to open reading frames of the expression clones by Gateway LR reaction. After polymerase chain reaction amplification and *in vitro* transcription, translation was performed using the wheat germ cell-free synthesis system. In the second step, we prepared WPAs by plotting synthesized proteins onto glass slides in an array format. WPAs were treated with serum samples derived from diseased patients or HCs. Autoantibodies were detected by fluorochrome-conjugated anti-human IgG Ab. In the third step, autoantibody quantification was performed based on the fluorescent values. Analysis of acquired high-dimensional autoantibody profiles was conducted by multiple omics-based approaches. ORF: open reading frame.

Figure 2. Identification of disease-specific autoantibodies.

(A) Box plots that show SAL in each condition. NS: P > 0.01, *: P < 0.01, ***: P < 0.0001. **(B)** Volcano plots that illustrate differentially elevated autoantibodies within each condition. Red horizontal dash lines indicate *P* values = 0.01. Red vertical dash lines indicate Log2 Fold Change (Disease/HC) = **±** 1. **(C)** Venn diagram that demonstrates the subsumptions among disease-specific autoantibodies. **(D)** UMAP plot that illustrates the distribution of disease-specific autoantibody profiles of each individual. **(E)** Heat map that shows the result of enrichment analysis targeting the genes responsible for the proteins targeted by such disease-specific autoantibodies. **(F)** Circos plot that depicts the overlap of the gene lists responsible for the proteins targeted by the disease-specific autoantibodies at the biological function level.

Figure 3. Autoantibodies highlighted in each machine learning model. Autoantibodies that are mostly highlighted according to feature importance in two-class **(A)**, three-class **(B)**, and multi-class **(C)** classifications. Correlograms depict correlations, showcasing the connection between the highest-ranked autoantibodies in two-class **(D)**, three-class **(E)**, and multi-class **(F)** classifications. The correlation strength is denoted by Spearman's rho on the color scale. Circle sizes represent the significance of the p-values, with only those with $P < 0.01$ being displayed. Radar charts present the average normalized quantities of the most important autoantibodies in each model, with line colors distinguishing between different disease categories in two-class **(G)**, three-class **(H)**, and multi-class **(I)** classifications.

Figure 4. COVID-19 signature of autoantibody landscape. (A) The heatmap's columns display the serum autoantibody concentrations highlighted in the multi-class classification using XGBoost. **(B)** PCA graph plots individual participants as points, with color coding to differentiate among various disease classes. **(C)** The loading diagram illustrates the contributions to PC1 and PC2, with I, II, and III marking the clusters defined in (A). **(D)** The bar graphs show the loadings of each autoantibody on PC1 and PC2. **(E)** A box plot presents the serum levels of anti-BCORP1 Abs in the subjects. **(F)** Another box plot indicates the serum levels of anti-KAT2A Abs in the subjects. Red vertical dash lines indicate mean + 2SD in HC.

Figure 5. Longitudinal change of humoral immune response in COVID-19. (A) This box plot outlines the serum concentrations of IgG antibodies against N, S, or RBD in patients with COVID-19 at two intervals: "early" signifies within 10 days of symptom onset, and "late" refers to 11-20 days after symptoms appear. A red dashed line marks the threshold for a positive test result. ***: $P < 0.0001$. **(B)** These box plots demonstrate the SAL in patients with COVID-19 during the "early" and "late" time points. NS: $P > 0.01$. **(C)** The volcano plot highlights biomarkers that are significantly increased (in red) or decreased (in blue) over time in patients with COVID-19. **(D)** A Venn diagram illustrates the overlap between autoantibodies that changed over time and those specific to COVID-19. **(E)** The correlogram visualizes the relationships between the overlapping autoantibodies that either increased over time or are specific to COVID-19, with the color scale indicating the strength of correlation according to Spearman's rho and circle sizes depicting the significance of p-values, focusing on those with $P < 0.01$. **(F)** These box plots depict the time-based evolution of serum levels of anti-BCORP1 and anti-KAT2A antibodies in COVID-19 patients, categorized by disease severity. **(G)(H)** The scatter plots illustrate the correlation between serum levels of anti-BCORP or anti-KAT2A Abs and IgG antibodies against the COVID-19 components at different time points, as well as their progression over time. The red lines

and the surrounding shaded areas indicate the regression line and the 95% confidence interval, respectively.

Supplementary Figure 1. The sum of autoantibody levels by sex and age. (A) The sum of autoantibody levels (SAL) in males. **(B)** SAL in females. **(C)** SAL for age < 50 years old. **(D)** SAL for age >= 50 years old.

Supplementary Figure 2. Autoantibodies to cytokines or their receptors. (A) The heatmap's columns display the serum autoantibody concentrations targeting cytokines in each subject evaluated by our proteome-wide autoantibody screening. **(B)** The heatmap's columns display the serum autoantibody concentrations targeting cytokine receptors in each subject evaluated by our proteome-wide autoantibody screening. **(C)** A box plot presents the serum levels of anti-interferon alpha 2 (IFNA2) Abs in the subjects. **(D)** Another box plot indicates the serum levels of anti-interferon alpha 4 (IFN4A) Abs in the subjects.

Supplementary Figure 3. Feature importance of top highlighted autoantibodies in other candidate machine learning frameworks. (A) Simple linear regression. **(B)** Ridge regression. **(C)** Logistic regression with normalization. **(D)** Logistic regression with standardization. **(E)** SVM with normalization. **(F)** SVM with standardization. **(G)** LightBGM. **(H)** Random Forest.

Supplementary Figure 4. Serum levels of anti-BCORP1 and anti-KAT2A Abs by sex and age. (A) Serum levels of anti-BCORP1 Abs by sex. F: female, M: male. **(B)** Serum levels of anti-BCORP1 Abs by age. **(C)** Serum levels of anti-KAT2A Abs by sex. **(D)** Serum levels of anti-KAT2A Abs by age. Red vertical dash lines indicate mean + 2SD in HC.

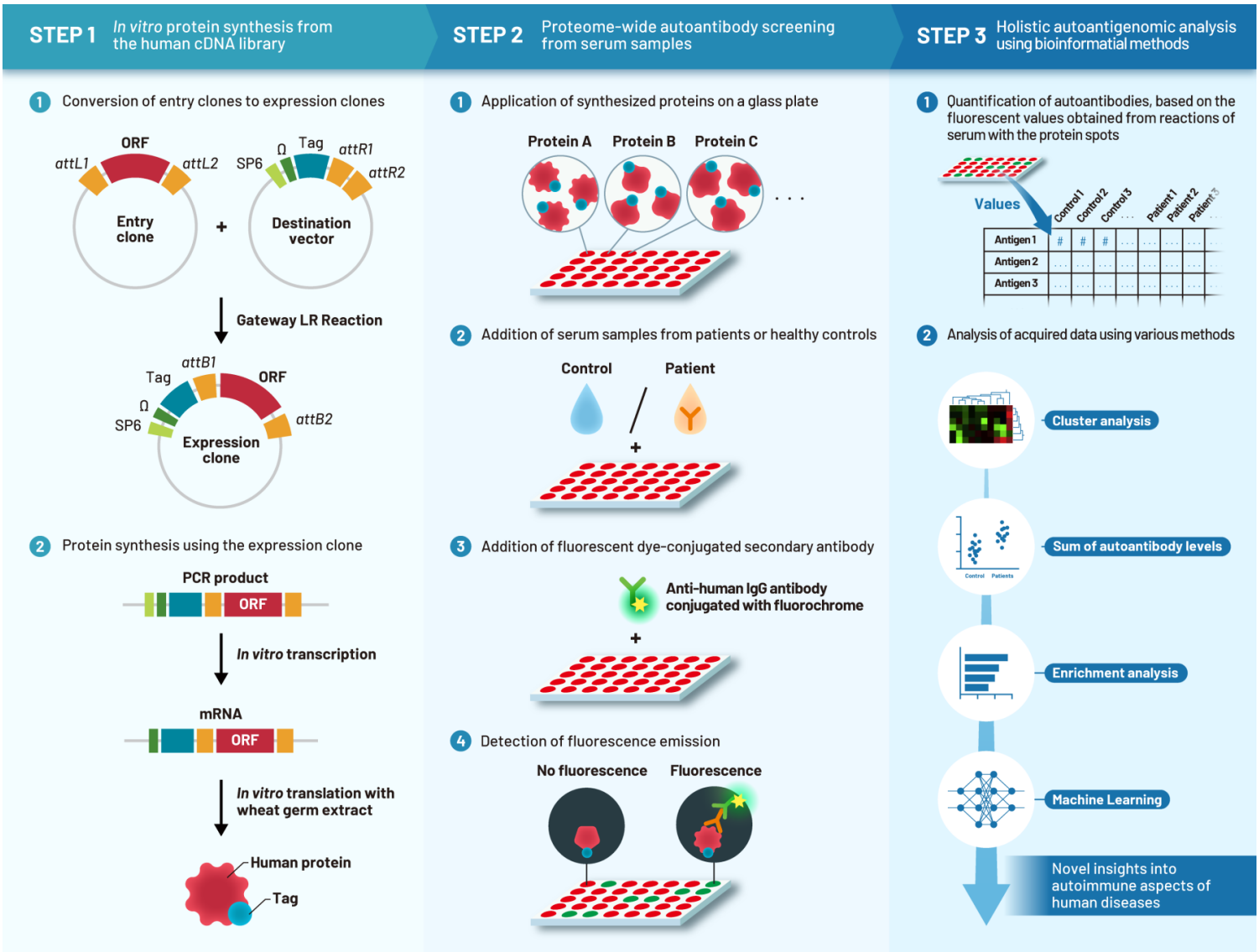

Matsuda KM et al.
Figure 1

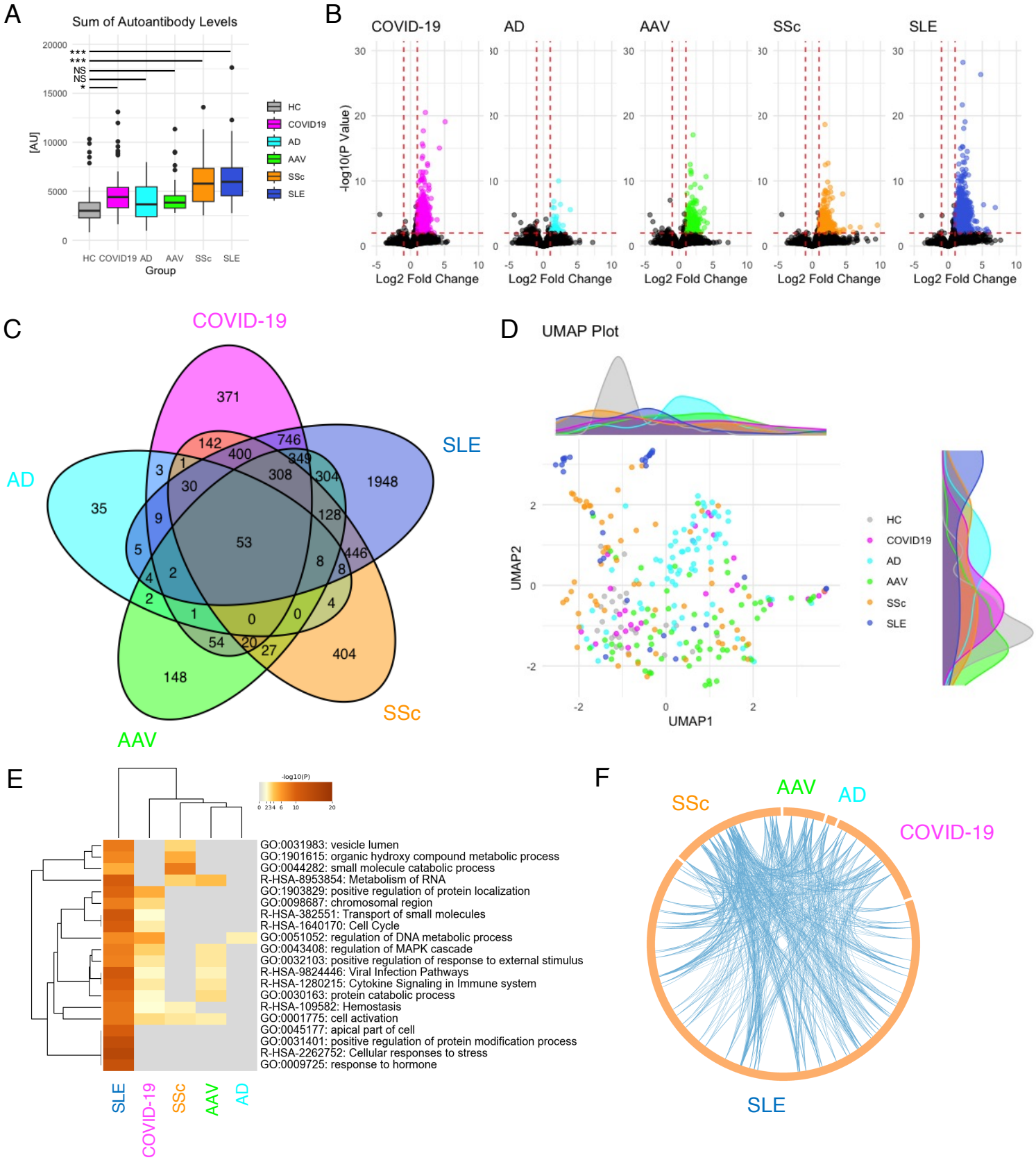

Matsuda KM et al.
Figure 2

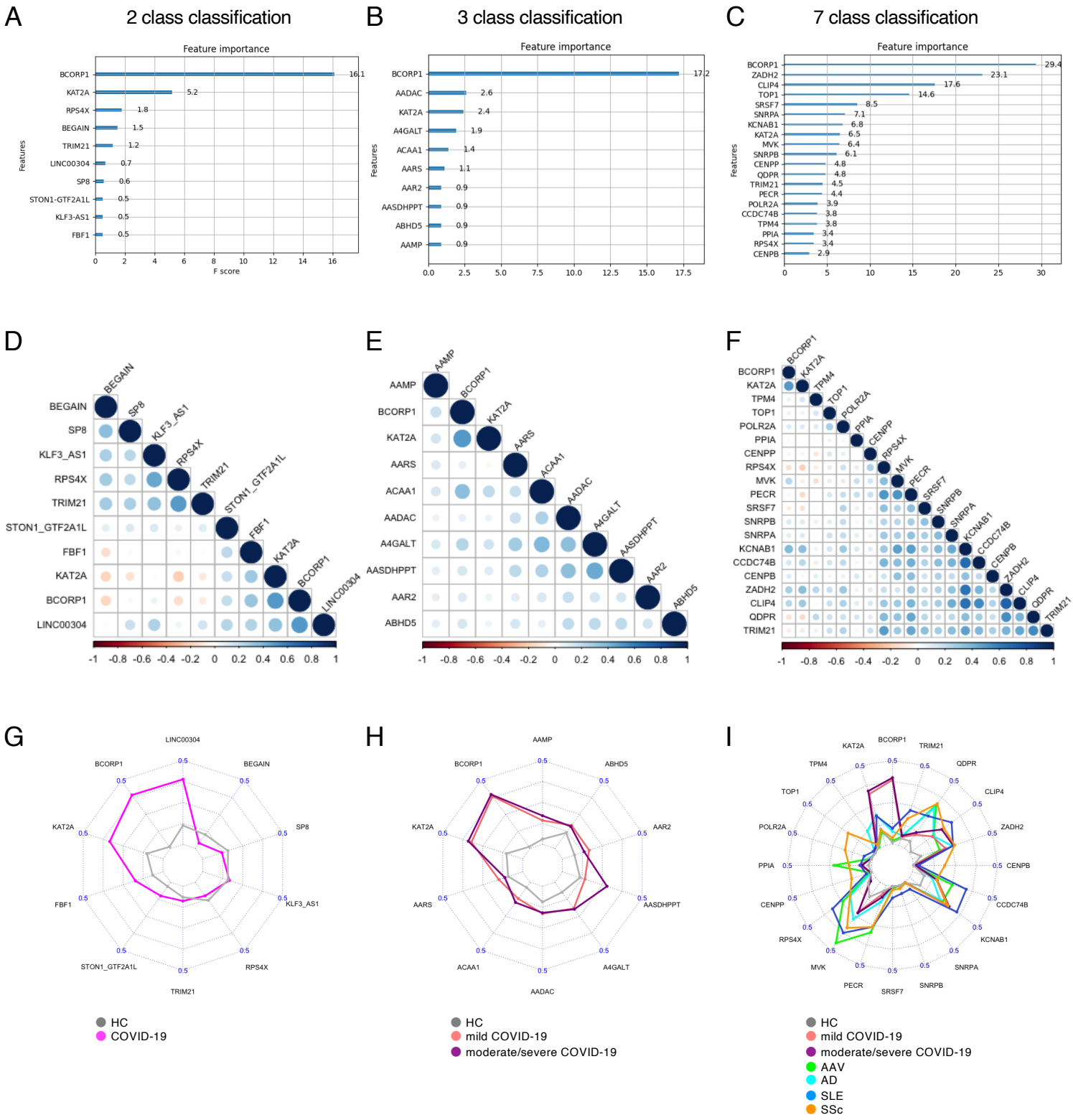

Matsuda KM et al.
Figure 3

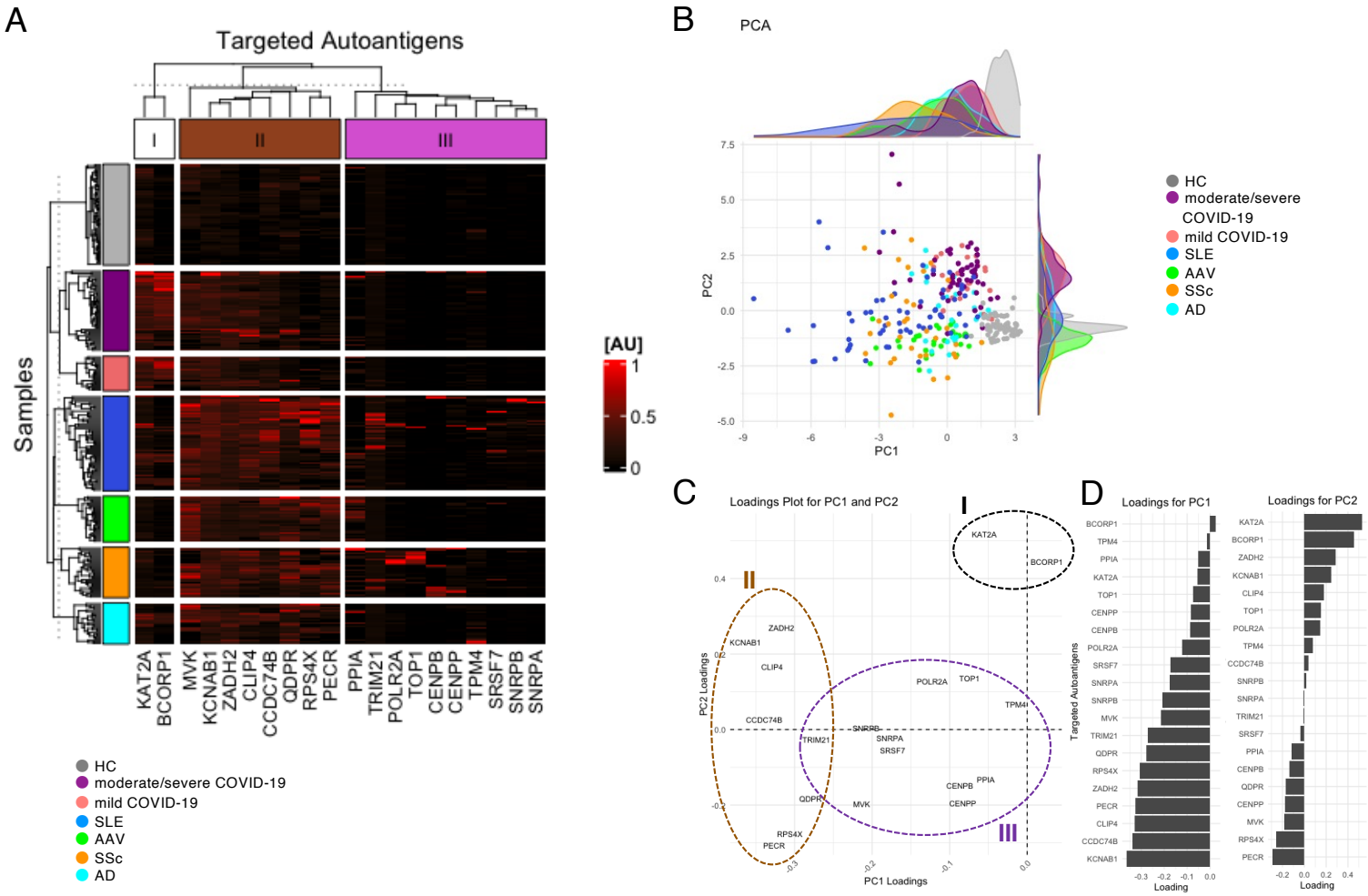

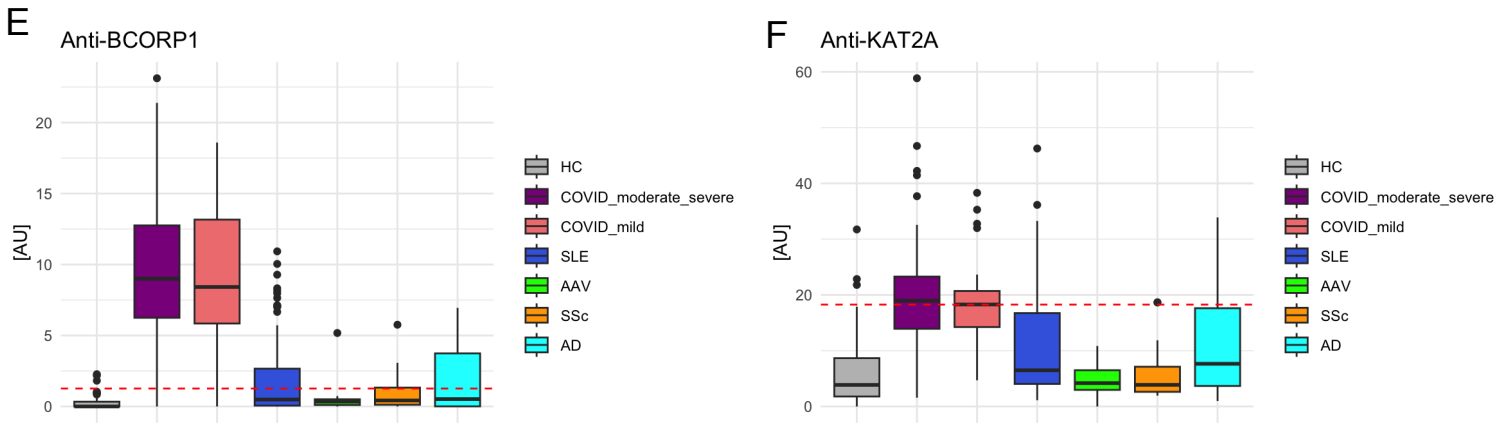

Matsuda KM et al.
Figure 4

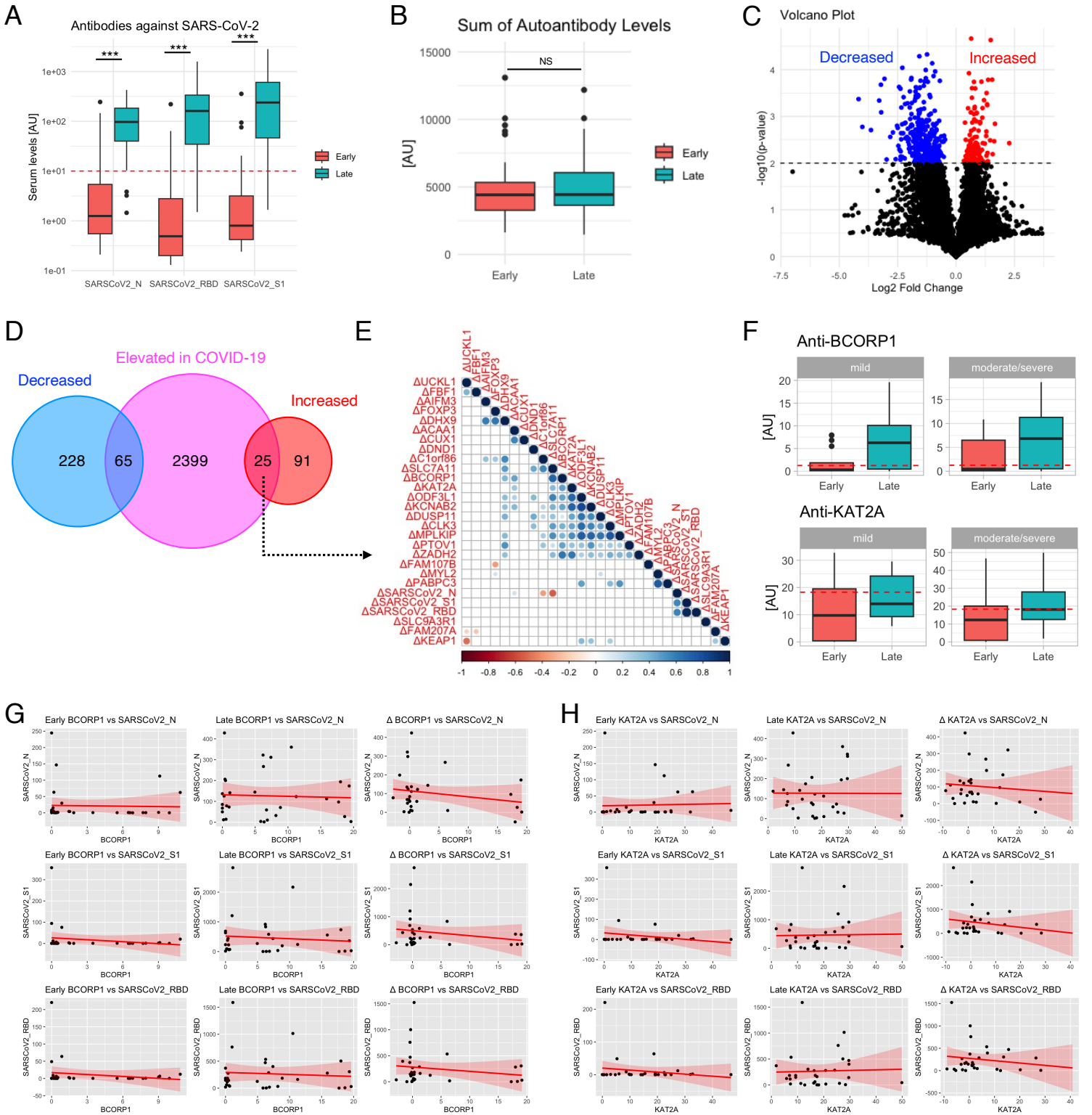

Matsuda KM et al.
Figure 5